THE JOURNAL OF BIOLOGICAL CHEMISTRY
Vol. 279, No. 38, Issue of September 17, pp. 40204–40208, 2004
Printed in U.S.A.

EXHIBIT B

High Resolution Crystal Structure of Human Rab9 GTPase

A NOVEL ANTIVIRAL DRUG TARGET*

Received for publication, June 24, 2004, and in revised form, July 16, 2004
Published, JBC Papers in Press, July 19, 2004, DOI 10.1074/jbc.M407114200

Liqing Chen‡§, Enrico DiGiammarino‡§, Xiaoyin E. Zhou‡§, Yujun Wang‡§, Diana Toh‡, Thomas W. Hodge¶, and Edward J. Meehan‡§‖

From the ‡Laboratory for Structural Biology, §Department of Chemistry, Graduate Programs of Biotechnology, Chemistry and Materials Science, University of Alabama in Huntsville, Huntsville, Alabama 35899 and ¶National Center for HIV, STD, and TB Prevention, Centers for Disease Control and Prevention, Atlanta, Georgia 30333

Rab GTPases and their effectors facilitate vesicular transport by tethering donor vesicles to their respective target membranes. Rab9 mediates late endosome to trans-Golgi transport and has recently been found to be a key cellular component for human immunodeficiency virus-1, Ebola, Marburg, and measles virus replication, suggesting that it may be a novel target in the development of broad spectrum antiviral drugs. As part of our structure-based drug design program, we have determined the crystal structure of a C-terminally truncated human Rab9 (residues 1–177) to 1.25-Å resolution. The overall structure shows a characteristic nucleotide binding fold consisting of a six-stranded β-sheet surrounded by five α-helices with a tightly bound GDP molecule in the active site. Structure-based sequence alignment of Rab9 with other Rab proteins reveals that its active site consists of residues highly conserved in the Rab GTPase family, implying a common catalytic mechanism. However, Rab9 contains seven regions that are significantly different in conformation from other Rab proteins. Some of those regions coincide with putative effector-binding sites and switch I and switch II regions identified by structure/sequence alignments. The Rab9 structure at near atomic resolution provides an excellent model for structure-based antiviral drug design.

Rab proteins, the largest subfamily of the Ras-like small GTPase superfamily, serve as molecular switches mediating tethering, docking, fusion, and motility of intracellular membranes (1). Rabs cycle between GTP-bound (on/active) and GDP-bound (off/inactive) conformations (2–4). The active form is stabilized by additional hydrogen bond interactions with the γ-phosphate of GTP mediated by serine residues in the phosphate-binding loop and switch I region as well as an extensive hydrophobic interface between the switch I and II regions (5, 6). The inactive conformation usually has displaced and mobile switch regions (3, 7). Biochemical and genetic studies of chimeric and mutant Rab proteins have identified several hypervariable regions, including the N and C termini and the α3/β5 loop, that play an important role in determining functional specificity (8, 9).

The Rab9 GTPase is localized predominantly to late endosomes and is required for the transport of mannose 6-phosphate receptors from endosomes to the trans-Golgi network (10, 11). Rab9 facilitates vesicular transport by pairing with its cognate Rab effector P40 (12). Rab9 also interacts with the vesicle cargo selection protein TIP47, which has been shown to bind the cytoplasmic tail of the HIV[1] envelope glycoprotein subunit gp41 (13). By targeting Rab9 mRNA for degradation with small interfering RNA, Rab9 has just been identified to be a key cellular component for HIV-1, Ebola, Marburg, and measles virus replication,[2] suggesting that inhibitors of Rab9 function, if developed, might prove useful in the control of those viruses. As part of a new structure-based antiviral drug design program, we have determined the crystal structure of a C-terminally truncated human Rab9 (residues 1–177) to near atomic resolution of 1.25 Å.

EXPERIMENTAL PROCEDURES

Cloning and Expression—The gene for human Rab9 (GenBank™ accession number NM_004251) was obtained from the IMAGE clone collection (IMAGE ID number 4139714) through distribution by OpenBiosystems. A C-terminally truncated fragment coding for residues 1–177 (20.1 kDa) was PCR subcloned using primers 5′-G ACA GCT AGC ATG GCA GGC AAA TCA TCA CTT TTT AAA G-3′ and 5′-C ATG GAT CCT TCA GTC CTC CGT AGC AAG AAC TCT TC-3′ into the NheI/BamHI restriction sites of pET28b (Novagen); the resulting construct encodes for a Rab9-(1–177) protein product with an N-terminal His_6-containing fusion (MGSSHHHHHHSSGLVPRGSHMAS). The pET28-Rab9-(1–177) vector was transformed into *Escherichia coli* BL21(DE3) (Novagen), and overproduction of the fusion protein was induced at an $A_{600\ nm}$ of ~2.0 with 1 mM isopropyl-1-thio-β-D-galactopyranoside at 310 K for 2 h; the cells were harvested by centrifugation and frozen at 253 K.

Protein Purification—The cell pellet was resuspended in nickel buffer A (20 mM Tris, pH 8.0, 500 mM NaCl, 5 mM imidazole), lysed by sonication, and centrifuged at 20,000 × *g* for 20 min at 277 K. The soluble fraction was filtered through a 0.45-micron filter and applied to chelating Sepharose (Amersham Biosciences), which had been previously charged with 50 mM $NiSO_4$ and equilibrated with nickel buffer A. The column was then washed with nickel wash buffer (20 mM Tris-HCl, pH 8.0, 500 mM NaCl, 55 mM imidazole), and the His_6-Rab9-(1–177) fusion protein was eluted with nickel elution buffer (20 mM Tris-HCl, pH 8.0, 500 mM NaCl, 350 mM imidazole). The His_6-Rab9-(1–177) fusion protein was then dialyzed against Thr buffer (20 mM Tris-HCl, pH 8.4,

* This work was supported in part by National Science Foundation-Experimental Program to Stimulate Competitive Research, NASA, and a generous gift from an anonymous donor to the Laboratory for Structural Biology, University of Alabama in Huntsville. The costs of publication of this article were defrayed in part by the payment of page charges. This article must therefore be hereby marked "*advertisement*" in accordance with 18 U.S.C. Section 1734 solely to indicate this fact.

The atomic coordinates and structure factors (code 1WMS) have been deposited in the Protein Data Bank, Research Collaboratory for Structural Bioinformatics, Rutgers University, New Brunswick, NJ (http://www.rcsb.org/).

‖ To whom correspondence should be addressed. Tel.: 256-824-6533; Fax: 256-824-6349; E-mail: meehane@uah.edu.

[1] The abbreviations used are: HIV, human immunodeficiency virus; MES, 4-morpholineethanesulfonic acid; r.m.s., root mean square; Gpp(NH)p, guanosine-5′-(β,γ)-imidotriphosphate; Gppsp, 5′-guanosine-diphosphate-monothiophosphate.

[2] J. L. Murray, N. J. Morey, M. Yilla, J. Sheng, W. J. Bellini, M. W. Shaw, C.-C. Luo, A. Sanchez, D. H. Rubin, and T. W. Hodge, personal communications.

```
1 MAGKSSLFKVILLGDGGVGKSSLMNRYVTNKFDTQLFHTIGVEFL
        B1          H1
46 NKDLEVDGHFVTMQIWDTAGQERFRSLRTPFYRGSDCCLLTFSVD
    B2       B3          H2       B4
91 DSQSFQNLSNWKKEFIYYADVKEPESFPFVILGNKIDISERQVST
          H3                 B5
136 EEAQAWCRDNGDYPYFETSAKDATNVAAAFEEAVRRVLATEDRSD
          H4          B6          H5
181 HLIQTDTVNLHRKFKPSSSCC
```

FIG. 1. **Amino acid sequence of human Rab9 and assignment of its secondary-structure elements.** α-Helix and β-sheet regions defined by the crystal structure are *underlined* and *labeled* (α-helices starting with *H* and β-strands with *B*).

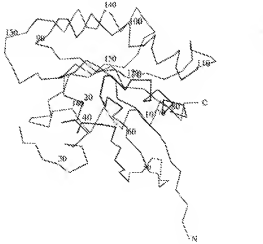

FIG. 2. **Stereoview of the Cα trace of Rab9.** Every 10th residue and both N and C termini are *labeled*. Residues 1, 35–38, and 176–177 are missing from the refined model and are not shown.

TABLE I
Summary of data collection, phasing, and refinement

Data and phasing statistics	
Space group	P_1
Unit cell: *a*, *b*, *c* (Å), α, β, γ (°)	38.40, 45.62, 51.22, 99.7, 107.2, 101.8
Wavelength (Å)	1.00
Resolution (Å)	1.25
Reflections (total/unique)	507,012/73,993
Completeness (%)	84.7 (39.9)[a]
I/σ	25.5 (2.3)[a]
$R(I)_{merge}$ (%)	6.3 (39.2)[a]
Molecular replacement model	Rab11a dimer
Refinement statistics	
Resolution range (Å)	10–1.25
Number of reflections	73,767
Number of atoms	Protein/GDP/water, 2662/56/508
R factors (%)	R_{work}/R_{free} 13.9/19.6
r.m.s. deviation of bonds	Length/angle distance, 0.013 Å/0.032 Å

[a] Values in parentheses are for the highest resolution shell.

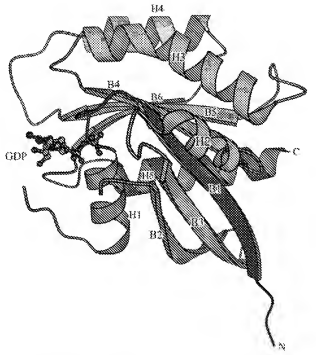

FIG. 3. **Ribbon representation of Rab9 structure.** A rainbow ramp color coding of *blue* to *red* is used to mimic chain trace from the N terminus to the C terminus. Both termini and the secondary structure elements are *labeled*. GDP in the active site is shown in *ball-and-stick* formation. *Gray*, carbon atoms; *blue*, nitrogen atoms; *red*, oxygen atoms; *purple*, phosphorus atoms.

150 mM NaCl, 2.5 mM $CaCl_2$) at 277 K, and precipitate was removed by centrifugation at 20,000 × *g* for 20 min at 277 K. To the soluble fraction, 1 unit of thrombin protease (Novagen) was added per milligram of fusion protein, and the His tag was removed by digestion for 4 h at 298 K (thrombin cleavage results in a Rab9a-(1–177) protein with an N-terminal GSHMAS extension). The thrombin cleavage reaction was diluted (1:3, v/v) with 20 mM MES, pH 6.5, and applied to Q-Sepharose (Amersham Biosciences), which had been previously equilibrated with Q buffer A (20 mM MES, pH 6.5, 50 mM NaCl). Native Rab9-(1–177) was eluted from Q-Sepharose with a 50–750 mM NaCl linear gradient in MES, pH 6.5; fractions containing native Rab9-(1–177) were identified by denaturing gel electrophoresis and pooled. The pooled Q fractions were then further purified by gel filtration on Sephacryl S-200 (Amersham Biosciences) in MES, pH 6.5, 150 mM NaCl; fractions containing Rab9-(1–177) were pooled and concentrated by ultrafiltration.

Crystallization and Data Collection—The stock protein solution used for crystallization contained 20 mM MES buffer, pH 6.5, and 150 mM sodium chloride with a protein concentration of 10 mg/ml. Crystals were grown at 277 K by the hanging-drop vapor diffusion method with 100 mM sodium acetate buffer, pH 5.0, 5% (v/v) polyethylene glycol 4000 as

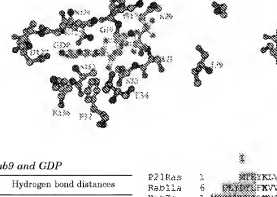

FIG. 4. **Stereoview of the active site showing the interactions between Rab9 and GDP.** *Gray*, carbon atoms; *blue*, nitrogen atoms; *red*, oxygen atoms; *purple*, phosphorus atoms. The bonds in GDP are colored *green*.

TABLE II
Hydrogen bonds between Rab9 and GDP

Rab9 atoms	GDP atoms	Hydrogen bond distances
		Å
Monomer A		
Gly-17 N	O1B	2.83
Gly-19 N	O3A	3.13
Lys-20 N	O2B	2.85
Lys-20 NZ	O2B	2.81
Ser-21 N	O3B	2.91
Ser-22 N	O1A	2.84
Ser-22 OG	O1A	2.68
Thr-34 OG1	O3[a]	3.02
Thr-34 OG1	O2[a]	3.05
Lys-125 NZ	O4[a]	3.04
Asp-127 OD1	N1	2.82
Asp-127 OD2	N2	2.83
Ala-155 N	O6	2.86
Monomer B		
Gly-17 N	O1B	2.89
Gly-19 N	O3A	3.13
Gly-19 N	O2B	3.02
Lys-20 N	O2B	2.88
Lys-20 NZ	O2B	2.75
Ser-21 N	O3B	2.96
Ser-22 N	O1A	2.93
Ser-22 OG	O1A	2.70
Thr-34 O	O2[a]	2.50
Asn-124	N7	3.17
Lys-125 NZ	O4[a]	2.99
Asp-127 OD1	N1	2.72
Asp-127 OD2	N2	2.83
Ala-155 N	O6	2.82

[a] Denotes atoms from sugar rings.

crystallization solution. Crystals formed in space group P_1 with a = 38.40 Å, b = 45.62 Å, c = 51.22 Å, α = 99.8°, β = 107.2°, and γ = 101.8° and contained two monomers in the unit cell. X-ray diffraction data to 1.25-Å resolution were collected at beamline 22-ID in the facilities of the South East Regional Collaborative Access Team at the Advanced Photon Source, Argonne National Laboratory. The statistics for data collection and processing are summarized in Table I.

Structure Determination and Refinement—The orientation and position of the Rab9 dimer in the P_1 unit cell were determined using the molecular replacement protocols in Crystallography & NMR System (14) starting from the structure of Rab11a (PDB code 1OIV (15)) as the search model. The composite omit map was calculated to guide electronic density fitting of the model. Energy-restrained crystallographic refinement was carried out with maximum likelihood algorithms implemented in Crystallography NMR software (14). Refinement proceeded through several cycles in combination with manual checking by the program O (16). The addition of two GDPs and 473 water molecules and refinement up to 1.25 Å resulted in R and R_{free} values of 0.213 and 0.232, respectively. Further refinement was continued with SHELX-97 (17) by subjecting the structure to cycles of isotropic conjugate gradient least squares refinement, then tightly restrained anisotropic displacement parameters were introduced and refined. The final refinement cycle resulted in R/R_{free} values of 0.139/0.196. The final model contains residues 2–34 and 39–175 of monomer A, residues 5–34, 39–110, and 115–175 of monomer B, and 2 GDP molecules plus 508 water molecules. The phasing and refinement statistics are summarized in Table I.

Protein Fold Analysis—Secondary structure elements were defined by the hydrogen-bonding patterns in combination with visual inspection. The Dali algorithm of comparing protein domain structures by alignment of distance matrices was used to search for structural homologues of Rab9 and also used for structure-based sequence alignment (18, 19). Ribbon diagrams were prepared by the program MOLSCRIPT (20).

FIG. 5. **Structure-based sequence alignment of Rab9 with the most similar structures.** The sequence number for the first residue of each line is indicated on the *left*. The positions of the secondary structural elements in Rab9 are indicated by *underlining* the sequence and *labeling* as in Fig. 1. Residues that are highly conserved in the Rab GTPase family are indicated in *boldface type*. Residues that are known to contact GDP in protein-GDP complex structures are indicated in *red*. Additional residues that would interact with the γ-phosphate in protein-GTP analog complex structures are shown in *purple*. The seven regions that show high degree of conformational variation among the superimposed structures (see Fig. 6) are highlighted in *gold* and *labeled*. See Table III for protein abbreviations and references.

RESULTS

Structure Determination—The human Rab9 variant we used for crystal structure determination included residues 1–177, lacking its last 24 residues (Fig. 1). Known as the C-terminal hypervariable region, the amino acid sequence of this region in Rab9 is poorly conserved with respect to other Rab proteins. Therefore, we excluded the C-terminal 24 residues from our cloning and crystallographic studies. We will refer below to this truncated form of the protein as Rab9.

Rab9 bound to GDP was crystallized, and its structure was determined by molecular replacement (Table I). The structure was refined against 1.25-Å resolution data, making it one of the highest resolution structures in the Rab protein family. Both N and C termini (residues 1 and 176–177 of monomer A and residues 1–4 and 176–177 of monomer B) and some loop re-

TABLE III
Alignment statistics of Rab9 with structurally similar proteins
Statistics were produced using the Dali algorithm (18, 19).

Protein name	Protein Data Bank code	Z[a]	RMSD[b]	LALI[c]	LSEQ2[d]	IDE[e]	Ref.
						%	
GDP-bound Rab9	1WMS	35.3	0.0	168	168	100	This paper
Gpp(NH)p-bound Ypt7p	1KY2	26.6	2.0	167	180	53	22
Gppsp-bound Rab11a	1OIW	25.4	1.4	158	166	41	15
Gpp(NH)p-bound p21Ras	1CTQ	25.2	1.6	161	166	31	21
GDP-bound Rab11a	1OIV	25.1	1.6	161	168	43	15
GDP-bound Ypt7p	1KY3	24.9	1.5	153	162	54	22
Gpp(NH)p-bound Sec4	1G17	24.7	1.6	159	168	38	7
Gpp(NH)p-bound Rab5a	1N6H	24.2	1.8	160	167	38	23
Gpp(NH)p-bound Rab5c	1HUQ	24.0	1.8	159	164	39	24
GDP-bound Sec4	1G16	23.3	1.5	150	156	35	7
Gpp(NH)p-bound Ypt51	1EK0	23.2	1.8	159	168	40	6

[a] Z-score, strength of structural similarity in standard deviations above expected.
[b] Positional root mean square deviation of superimposed Cα atoms in Å.
[c] Total number of equivalent residues.
[d] Length of the entire chain of the equivalent structure.
[e] Percentage of sequence identity over equivalent positions.

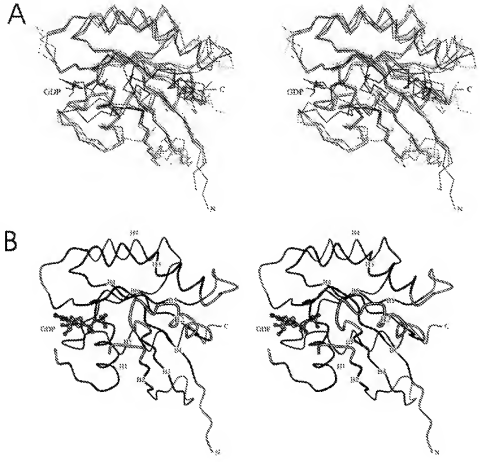

FIG. 6. **Structure comparison.** *A*, stereoview of structural alignment of Rab9 with three GTPases. The Cα backbone in GDP-bound Rab9 (*black*, residues 2–34 and 39–175) is superimposed with GDP-bound Ypt7p (*green*, residues 7–37, 41–46, 77–181, and Protein Data Bank accession number 1KY3), GDP-bound Rab11a (*blue*, residues 6–175, and Protein Data Bank accession number 1OIV), and Gpp(NH)p-bound p21Ras (*red*, residues 1–166, Protein Data Bank accession number 1CTQ). For clarity, only the GDP molecule in the active site of Rab9 structure is shown and colored *black*. Both N and C termini of Rab9 are *labeled*. *B*, stereoview of Rab9 backbone structure highlighting the seven hypervariable regions shown in *yellow* while the rest are shown in *black*. Both termini and the secondary structure elements are *labeled*. GDP in the active site is shown in *ball-and-stick* formation. *Gray*, carbon atoms; *blue*, nitrogen atoms; *red*, oxygen atoms; *purple*, phosphorus atoms.

gions (residues 34–38 of both monomers and residues 111–114 of monomer B) were disordered and could not be seen in the experimental electron density map. The final refined model, which includes residues 2–34 and 39–175 of monomer A, residues 5–34, 39–110, and 115–175 of monomer B, 2 GDP molecules, and 508 ordered water molecules, has a working R value of 0.139 and a free R value of 0.196. The stereochemistry is excellent with r.m.s. deviations for bond lengths and angle distances of 0.013 Å and 0.032 Å, respectively (Table I). The Ramachandran plot statistics showed that 93.2% of the backbone dihedral angles were in the most favored regions, 6.8% in the additional allowed regions, and none of the non-glycine residues were in the disallowed regions. The two crystallographically unique Rab9 molecules in the crystal unit cell have almost identical structures with the r.m.s. deviation between the 161 equivalent Cα atoms of 0.40 Å. We will use monomer A in our description of Rab9 structure.

Overall Structure of Rab9—Like other members of the Rab GTPase family, Rab9 adopts a classical nucleotide binding fold consisting of a six-stranded β-sheet surrounded by five α-helices (Figs. 2 and 3). The five α-helices (H1-H5) and six β-strands (B1-B6) connect with a B1-H1-B2-B3-H2-B4-H3-B5-H4-B6-H5 topology containing 30.5% (54/177) α-helix, 28.8% (51/177) β-sheet, 37.3% (66/177) turn/loop, and 3.4% (6/177) other (Figs.

1 and 3). The six β-strands arrange in the order of B2-B3-B1-B4-B5-B6, forming a mostly parallel β-sheet except that B2 is antiparallel to the rest in strand direction.

Active Site Structure—The crystal structure reported here contains a tightly bound GDP molecule in the active site (Figs. 3 and 4). Rab9 residues making hydrogen bonds with GDP include Gly-17, Gly-19, Lys-20, Ser-21, Ser-22, Thr-34, Asn-124, Lys-125, Asp-127, and Ala-155 (Table II, Fig. 4, and as shown by the color *red* in Fig. 5). These residues together with Gly-16, Val-18, Phe-32, Ile-126, and Lys-156 form a tight binding pocket accommodating the GDP molecule. There are more than a dozen hydrogen bonds formed between Rab9 and GDP, indicating a strong binding affinity of Rab9 for GDP. This is supported by the observation that the GDP molecule has been kept inside the active site throughout Rab9 purification, that is it comes naturally bound to Rab9 from the cell culture. Residues Thr-39 and Gly-65 are highly conserved in the Rab GTPase family and are predicted to interact with the γ-phosphate of GTP in the active state of Rab9.

DISCUSSION

Structure Comparison—The overall structure of Rab9 is very similar to the prototype Ras protein p21Ras (21) and several Rab proteins (Table III). Among those, Rab9 has the highest sequence identity with Ypt7p (54% over 153 equivalent positions), followed by Rab11a (43% over 161 equivalent positions). The structural similarity Z-scores (18, 19) range from 26.6 to 23.2 with r.m.s. deviations of equivalent positions in the range of 1.4–2.0 Å. Structure-based sequence alignment reveals that the active site of Rab9 consists of residues highly conserved in the Rab GTPase family (Fig. 5), implying a common catalytic mechanism. However, Rab9 contains seven hypervariable regions that are significantly different in conformation from other Rab proteins (Figs. 5 and 6). Some of those regions coincide with putative effector-binding sites and conformational switch I and switch II regions identified by earlier crystallographic studies of other Rab proteins. Regions II and IV correspond to the switch I and switch II, respectively, whereas regions I, V, and VII correspond to the three effector-binding sites/complementary determining regions. These seven hypervariable regions in Rab9 structure may serve as sites for antiviral drug binding and provide an excellent target for structure-based drug design and development.

Acknowledgments—Use of the Advanced Photon Source was supported by the United States Department of Energy, Office of Science, Office of Basic Energy Sciences, under contract number W-31-109-Eng-38. We thank J. Looger of University of Alabama in Huntsville for technical assistance in computer programs and the staff of the South East Regional Collaborative Access Team beamline 22ID at the Advanced Photon Source for help with data collection. We are also grateful to OpenBiosystems Inc. for the free gift of Rab9 cDNA.

REFERENCES

1. Pfeffer, S. R. (2001) *Trends Cell Biol.* **11**, 487–491
2. Pfeffer, S. R. (1994) *Curr. Opin. Cell Biol.* **6**, 522–526
3. Bourne, H. R., Sanders, D. A., and McCormick, F. (1991) *Nature* **349**, 117–127
4. Sprang, S. R. (1997) *Annu. Rev. Biochem.* **66**, 639–678
5. Dumas, J. J., Zhu, Z., Connolly, J. L., and Lambright, D. G. (1999) *Structure Fold Des.* **7**, 413–423
6. Esters, H., Alexandrov, K., Constantinescu, A. T., Goody, R. S., and Scheidig, A. J. (2000) *J. Mol. Biol.* **298**, 111–121
7. Stroupe, C., and Brunger, A. T. (2000) *J. Mol. Biol.* **304**, 585–598
8. Brongwald, P., and Novick, P. (1993) *Nature* **362**, 560–563
9. Stenmark, H., Valencia, A., Martinez, O., Ullrich, O., Goud, B., and Zerial, M. (1994) *EMBO J.* **13**, 575–583
10. Lombardi, D., Soldati, T., Riederer, M. A., Goda, Y., Zerial, M., and Pfeffer, S. R. (1993) *EMBO J.* **12**, 677–682
11. Riederer, M. A., Soldati, T., Shapiro, A. D., Lin, J., and Pfeffer, S. R. (1994) *J. Cell Biol.* **125**, 573–582
12. Díaz, E., Schimmoller, F., and Pfeffer, S. R. (1997) *J. Cell Biol.* **138**, 283–290
13. Blot, G., Janvier, K., Le Panse, S., Benarous, R., and Berlioz-Torrent, C. (2003) *J. Virol.* **77**, 6931–6945
14. Brunger, A. T., Adams, P. D., Clore, G. M., DeLano, W. L., Gros, P., Grosse-Kunstleve, R. W., Jiang, J. S., Kuszewski, J., Nilges, M., Pannu, N. S., Read, R. J., Rice, L. M., Simonson, T., and Warren, G. L. (1998) *Acta Crystallogr. Sect. D Biol. Crystallogr.* **54**, 905–921
15. Pasqualato, S., Senic-Matuglia, F., Renault, L., Goud, B., Salamero, J., and Cherfils, J. (2004) *J. Biol. Chem.* **279**, 11480–11488
16. Jones, T. A., Zou, J. Y., Cowan, S. W., and Kjeldgaard, M. (1991) *Acta Crystallogr. Sect. A* **47**, 110–119
17. Sheldrick, G. M., and Schneider, T. R. (1997) *Methods Enzymol.* **227**, 319–343
18. Holm, L., and Sander, C. (1993) *J. Mol. Biol.* **233**, 123–138
19. Holm, L., and Sander, C. (1998) *Proteins* **33**, 88–96
20. Kraulis, P. J. (1991) *J. Appl. Crystallogr.* **24**, 946–950
21. Scheidig, A. J., Burmester, C., and Goody, R. S. (1999) *Structure Fold Des.* **7**, 1311–1324
22. Constantinescu, A. T., Rak, A., Alexandrov, K., Esters, H., Goody, R. S., and Scheidig, A. J. (2002) *Structure (Lond.)* **10**, 569–579
23. Zhu, G., Liu, J., Terzyan, S., Zhai, P., Li, G., and Zhang, X. C. (2003) *J. Biol. Chem.* **278**, 2452–2460
24. Merithew, E., Hatherly, S., Dumas, J. J., Lawe, D. C., Heller-Harrison, R., and Lambright, D. G. (2001) *J. Biol. Chem.* **276**, 13982–13988